

Eleventh U.S. National Conference on Earthquake Engineering

Integrating Science, Engineering & Policy June 25-29, 2018 Los Angeles, California

Structure-from-Motion based 3D mapping of landslides & fault rupture sites during 2016 Kaikoura earthquake reconnaissance

Zekkos, D.¹, Manousakis, J.², Athanasopoulos-Zekkos, A.³, Clark, M.⁴, Knoper, L.⁵, Massey, C.⁶, Archibald, G.⁷, Greenwood, W.⁸, Hemphill-Haley, M.⁹, Rathje, E.¹⁰, Litchfield, N.¹¹, Medwedeff, W.¹², Van Dissen, R.J.¹¹, Kearse, J.¹¹, Ries, W.¹¹, Villamor, P.¹¹& Langridge, R.M.¹¹

ABSTRACT

Following the November 14 2016 M_w7.8 Kaikoura earthquake, field expeditions were undertaken using Unmanned Aerial Vehicles (UAVs) to map 25 sites of scientific interest with a plan area of 7.2 km². A total of 23,172 images collected by the UAVs were used as input in Structure-from-Motion (SfM) to create 3D models of the target areas with a focus on landslides and fault rupture. Two sites are presented in more detail as examples of the data generated; a section of the Kekerengu fault that ruptured during the earthquake, and the Limestone Hills landslide. The sites were mapped at high resolution with ground sampling distance that varied from 0.5 to 7.0 cm/pixel. The developed SfM models were compared to 1-m aerial LiDAR data and the results were found to be comparable. However, the higher resolution of the SfM digital surface model (DSM), paired with the imagery facilitated more detailed interpretations, highlighting the usefulness of the UAV-enabled SfM as a mobile and effective technique for documenting perishable post-earthquake reconnaissance data.

¹ Associate Professor, Dept. of Civil and Environmental Engineering, University of Michigan, 2350 Hayward Str. Ann Arbor, MI, 48109 (e-mail: zekkos@geoengineer.org)

² Geomatics Engineer, Elxis Group, Dimitressa 7-9 Athens, 115 28, Greece.

³ Associate Professor, Dept. of Civil and Environmental Engineering, University of Michigan, 2350 Hayward Str. Ann Arbor, MI, 48109

⁴ Associate Professor, Dept. of Earth & Environmental Science, University of Michigan, 2534 C. C. Little Building 1100 North University Avenue, Ann Arbor, MI 48109

⁵ Research Assistant, Dept. of Earth & Environmental Science, University of Michigan, 2534 C. C. Little Building,1100 North University Avenue, Ann Arbor, MI 48109

⁶ Engineering Geologist, GNS Science, New Zealand

⁷ Engineering Geological Surveyor, GNS Science, New Zealand

⁸ PhD student, Dept. of Civil and Environmental Engineering, University of Michigan, 2350 Hayward Str. Ann Arbor, MI, 48109

⁹ Professor, Dept. of Geology, Humboldt State University, 1 Harpst St., Arcata, CA 95521

¹⁰ Associate Professor, Dept. of Civil, Architectural, and Environm. Eng, 301 E. Dean Keeton St. Stop C1700, Austin, Texas 78712

¹¹ Fault Rupture Team, GNS Science, New Zealand

¹² PhD student, Dept. of Earth & Environmental Science, University of Michigan, 2534 C. C. Little Building 1100 North University Avenue, Ann Arbor, MI 48109

Introduction

The collection of high quality, perishable data following an earthquake is an important step in our efforts to learn from specific earthquake events. Thus, there is a need for mobile methodologies that can collect the data efficiently. One of the relatively more recent data acquisition methodologies that has been applied in post-earthquake reconnaissance is Structure-from-Motion (SfM). SfM is a photogrammetric and computer vision technique where overlapping imagery is collected commonly (but not necessarily) using Unmanned Aerial Vehicles (UAVs) and used as input to generate three dimensional photorealistic models of a target. The technique has previously been applied for reconnaissance purposes following the 2015 earthquake in Lefkada, Greece (Zekkos et al. 2017), 2015 earthquake in Nepal (Greenwood et al. 2015), 2014 Chile (Franke et al. 2017), and 2016 Kumamoto earthquake (Kayen et al. 2016).

In this contribution, the application of SfM to document primarily landslide and fault rupture sites following the November 14 2016 M_w 7.8 Kaikoura earthquake in New Zealand is presented. Emphasis is given on the ability of the technique to map not only the large (multi-meter) size aspects of the target features, but also the smaller-size features (sub-m) that are extremely time consuming to measure using conventional topographic mapping techniques. The SfM UAV—enabled models are then compared to aerial LiDAR data that have been collected by others to draw lessons about the mapping capabilities of the SfM technique.

Field Data Collection

A total of 25 sites were mapped using the Structure-from-Motion (SfM) technique in the south island of New Zealand. The sites were primarily fault rupture sites and landslides that occurred during the November 14 2016 M_w 7.8 Kaikoura earthquake, but also included other sites (such as an uplifted site and other sites). A summary of the sites mapped and information about them, including the achieved mapping resolution (expressed in terms of ground sampling distance), mean flight height and imagery collected is presented in Table 1. Figure 1 shows the location of the 25 sites.

The sites were mapped during two field expeditions: The first during November 23 to December 3 2016 that was part of the Geotechnical Extreme Event Reconnaissance (GEER) group reconnaissance, and the second one during March 28 to April 4 2017 as part of a subsequent field deployment by the University of Michigan.



Figure 1. Locations of mapped areas in northeast of south island using UAVs and SfM. Site IDs refer to Table 1. Larger bold font used for sites presented in more detail in this paper

Table 1. Site characteristics of mapped locations as part of this study.

Site	Site	Type *	Date dd/mm/yr	Area (km²)	Mean flight height (m)	GSD (cm / pixel)	# of Photos
S1	East Lane Kekerengu Fault 1	FR	23/11/16	0.200	56	3.15	408
S2	East Lane Kekerengu Fault 2	FR	23/11/16	0.371	90	3.87	892
S3	South of Glincoe Stream Landslide	FR & LS	26/11/16	0.186	90	4.33	287
S4	House at Bluff Station	FR	25/11/16	0.091	53	2.51	372
S5	Ben Moore Stream Kekerengu Fault 1	FR	24/11/16	0.122	62	2.72	369
S6	Ben Moore Stream Kekerengu Fault 3	FR	28/11/16	0.136	60	2.31	357
S7	Ben Moore Stream Kekerengu Fault 4	FR	28/11/16	0.166	67	3	377
S8	Ben Moore Stream Kekerengu Fault 5	FR	28/11/16	0.133	55	2.73	360
S9	Ben Moore Stream Kekerengu Fault 6	FR	28/11/16	0.103	55	2.65	381
S10	Ben Moore Stream Kekerengu Fault 7	FR	28/11/16	0.095	50	2.36	383
S11	Railway Line Kekerengu Fault	FR	23/11/16	0.101	50	2.54	378
S12	Clarence River Sea View (Seafront LS)	LS	1/12/16	1.420	135	5.27	1039
S13	Clarence River Little Nelson LS	LS	3/12/16	0.285	100	4.33	433
S14	Clarence River Limestone Hills LS	LS	3/12/16	0.492	94	3.73	610
S15	Goose Bay LS Dam	LS	29/11/16	0.521	150	5.92	358
S16	Leader Landslide	LS	28-30 /3/17	2.210	50-250	1.91-7.01	7815
S17	Leader Landslide	О	30/3/17	0.192	60	1.93	519
S18	Kaikoura Coast Uplift	О	31/3/17	0.015	20	0.57	956
S19	Puhi-Puhi River	LS	31/3/17	0.020	40	0.79	1396

S20	Near Waiau	FR	1/4/17	0.136	50	1.25	482
S21	Mt. Lyford Rec. Entrance	LS	1/4/17	0.010	~50	~1.25	399
S22	Road 70	LS	2/4/17	0.005	~50	~1.25	1823
S23	Road 70	О	2/4/17	0.002	~50	~1.25	508
S24	Road 7	О	3/4/17	0.169	60	1.69	571
S25	Farm north of Limestone Hills	LS	4/4/17	0.040	~50	~1.25	1699

*FR: Fault Rupture; LS: Landslide; O: Other.

Sites S1-S15 mapped by DJI Phantom 3 Pro. Sites S16-S25 mapped by DJI Phantom 4 Pro.

Two Unmanned Aerial Vehicles were used in field deployment: The DJI Phantom 3 Pro and the DJI Phantom 4 Pro. Their characteristics, as reported by the manufacturer are compared in Table 2. Both UAVs are small size and, thus, the approach followed is mobile and well-suited for post-earthquake response (Figure 2). Despite the reported 4 km flight range reported for Phantom 4 Pro, our experience was that the UAV could safely (without loss of signal) map areas that were at a radius less than 800 m. The team also noted a significant improvement in flight control for the Phantom 4 Pro compared to the Phantom 3 Pro during high wind conditions (e.g. ≥30 km/hr). For the collection of the imagery, for the most part, a lawn-mower type autonomous flight path was used with the camera in the nadir (i.e. facing downwards) position. However, in some cases, additional imagery was collected with the camera pointing in an oblique direction. In total, for the sites shown in Table 1, 7.2 km² (in plan area) were mapped, with a flight time of 1100 minutes, and a total of 23,172 images were collected and used to develop the SfM models.



Figure 2. Equipment used for UAV-enabled SfM mapping in New Zealand (missing from the photo are the GNSS receivers used for ground control points).

Analysis Methodology

SfM is a photogrammetric and computer vision technique that uses overlapping imagery to identify matching features in multiple images. Compared to a classic photogrammetric technique where

the location of the camera is known, in SfM a non-linear least-squares minimization technique is used to iteratively estimate the 3D relative location of both camera positions and object coordinates, and a sparse bundle adjustment is implemented to transform measured image coordinates to three dimensional points of the area of interest (Westoby et al. 2012). Subsequently, the 3D point cloud is densified beyond the identified features. Ground control points using GNSS measurements are then used to optimize the camera's internal and external parameters and to georefence the 3D point cloud to a specific coordinate system. Ground check points also measured using GNSS sensors are used to estimate model errors. Through post-processing, a digital surface model (DSM), and possibly a digital terrain model (DTM) and orthophotos are created. In this study the technique was implemented using the Pix4D and Agisoft Photoscan software.

Table 2: Characteristic	es of the UA	Vs used in this stud	v as reported by	DII (manufacturer)
radic 2. Characteristic	os of the OA	v o uocu iii uiio otuu	y as reported by	DJI (IIIaiiuiaciuici).

	Phantom 3 Pro	Phantom 4 Pro	
Flight time	< 23 min	< 28 min	
Speed	16 m/s	20 m/s	
Camera	12 MP / 4k video	20 MP / 4k video	
Flight control sensing	Vision Positioning (VP)	VP & StereoVision + Infrared for collision avoidance	
Range	<2000 m	4000+ m	
Navigation	GPS+GLONASS	GPS+GLONASS	

Results

Indicative results for two areas, one fault rupture (Kekerengu fault) and one landslide (Limestone Hills landslide) are presented subsequently.

Structure-from-Motion Mapping of Kekerengu Fault Rupture

Kekerengu fault is one of the active faults in the southeast corner of the Marlborough Fault System with a NE strike and slip rate of about 18-25 mm/yr (Van Dissen et al. 2016). During the November 14 2016 earthquake event, Kekerengu fault exhibited the largest onshore displacements with a 12 m dextral offset and 1-3 m vertical offset (Hamling et al. 2017, Kearse et al. 2018). Sites S1-S11 (listed in Table 1 and shown in Fig. 1) were mapped along the Kekerengu fault. Figure 3 shows the mapping result of sites S5-S8 along the Kekerengu fault. Fig. 3a is a perspective view of a lower resolution (average Ground Sampling Distance (GSD) of 20 cm) orthophoto draped on terrain. It also shows the ground control points and ground check points collected using GNSS receivers and used in camera optimization, georeferencing and error assessment for the model. The xyz Root Mean Square Error (RMSE) based on the check points is 16.7 cm. Fig. 3b is a Digital Surface Model (DSM) of the SfM model and Fig. 3c is a 1 m DSM from aerial LiDAR.

Figure 4 is a DEM of difference between the LiDAR DSM and the SfM DSM. The two DSMs are in excellent agreement with a mean difference of 0.02 m and a standard deviation of 0.23 m. The greatest differences (of approximately 6-8 m) are observed in areas of vegetation and along the electric posts and cables (shown as a poly-line in Fig. 4), which are features better captured by the LiDAR compared to the UAV. Although that is not a critical issue for the intended purpose of the mapping, it is interesting to note that the cables and electric posts were adequately

imaged in areas where two perpendicular lawn-mower type flight paths were conducted with the camera in an oblique position, but they were not well-imaged when one flight path with the camera in the nadir position was executed.

Also, of interest is the comparison between the DSM at a finer scale in order to investigate whether the SfM-generated DSM can be used to map the rupture characteristics. Fig 5a is a higher resolution view of the fault rupture. The full resolution 5 cm SfM-generated DSM is shown in Fig. 5c, while Fig. 5d shows the 1 m DSM based on LiDAR. It is evident that due to its higher resolution, the SfM-generated DSM can better depict detailed fracture and fault patterns of the fault rupture. In addition, the SfM-generated DSM is accompanied by an orthophoto, i.e., its pixels have RGB attributes, that facilitate the identification of the characteristics of the ground surface. This is evident in Fig. 5b, which is a topographic profile across the fault rupture. Both LiDAR and SfM-generated DSMs capture the overall geometry, however, the SfM-generated DSM better identifies the step-type elevation change along both sides of the fault and provides a means to measure the rupture's width and depth. This level of detail is not captured by the 1 m LiDAR-generated DSM. In addition, the SfM mapping was compared against field surveys collected with total station and/or RTK GPS at several locations and was found to be consistent within decimeter resolution. An example is shown in Fig. 6.

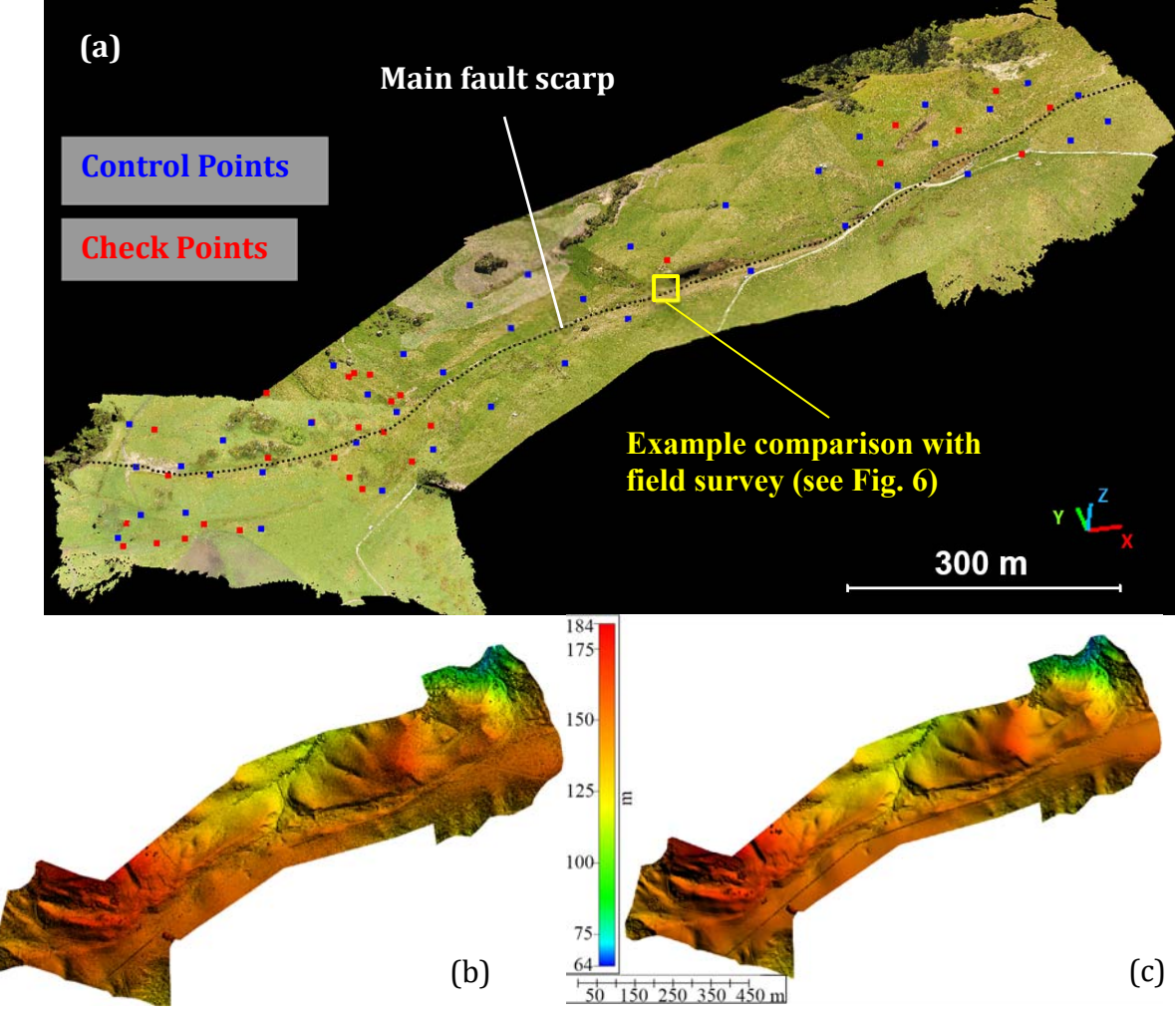


Figure 3 (a) 20 cm orthophoto using SfM; (b) DSM using SfM; and (c) DSM using LiDAR.

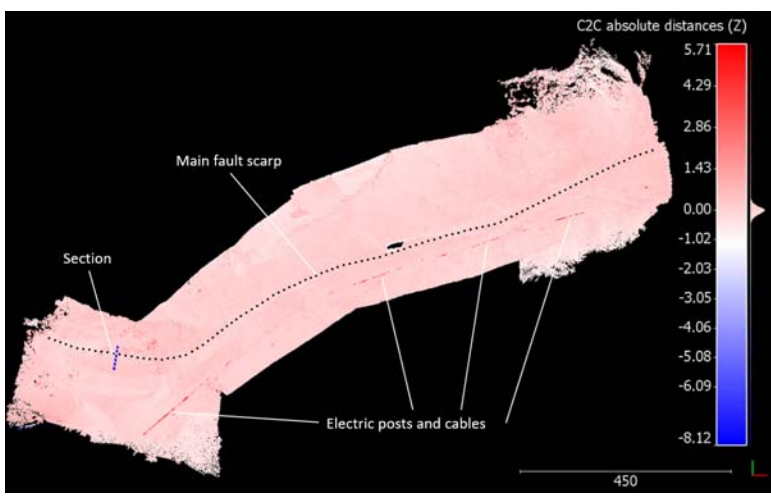


Figure 4. Digital Elevation Model (DEM) representing difference between LiDAR DSM and SfM DSM. The trace of the main scarp is shown. Also, the location of a section through the main scarp is shown and is presented in Figure 5.

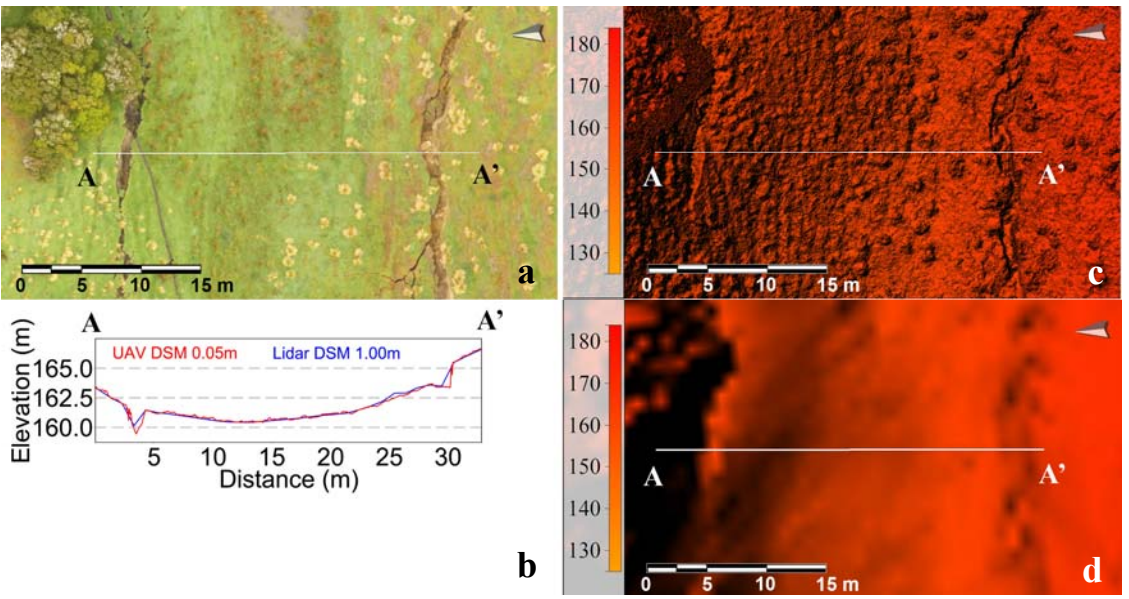


Figure 5. (a) SfM orthophoto of fault rupture at section location shown in Fig. 4; (b) Profile through rupture; (c) SfM 5-cm DSM; (d) LiDAR 1-m DSM

Structure-from-Motion Mapping of Limestone Hills Landslide

More than 10,000 landslides occurred during the Kaikoura earthquake event (Massey et al. 2017, Dellow et al. 2017). Among the larger landslides that occurred during the event is the Limestone Hills landslide that has a height of about 130 m (site S14 in Table 1) and its location is shown in Figure 1. Figure 7a shows an oblique view of the 3D model that was created using SfM, and also shows the 17 ground control points used in model development. The mean flight altitude was about 95 m and the area covered is 0.49 km². The average ground sampling distance of the model is 3.73 cm/pixel. A total of 610 images were used in model development and the xyz RMS error was 8.3 cm. The orthophoto of the SfM model is shown in Figure 7b and the SfM DSM is shown in Figure 7c. Figure 7d shows the 1-m LiDAR DSM, which visually can be assessed to be very similar to

the 20-cm SfM DSM. This is better illustrated in Figure 7e where the DEM of difference between the two DSMs is represented. Overall, differences between the DSMs are less than 1 m in elevation. Figure 7f shows cross-sections through the landslide mass. It is evident that for many practical purposes, e.g., volume estimation, and landslide stability analyses, the post-earthquake surface using LiDAR or SfM are identical. In addition, the 2012 LiDAR DSM that unfortunately covers a portion of the landslide only, is used to define the pre-earthquake geometry. It is shown for cross-section A-A' only (Fig. 7f) that illustrates the loss of mass near the crest and the deposition of material at the toe of the landslide. Based on this comparison, the landslide is estimated to have moved about 80 m in the horizontal direction during the earthquake.

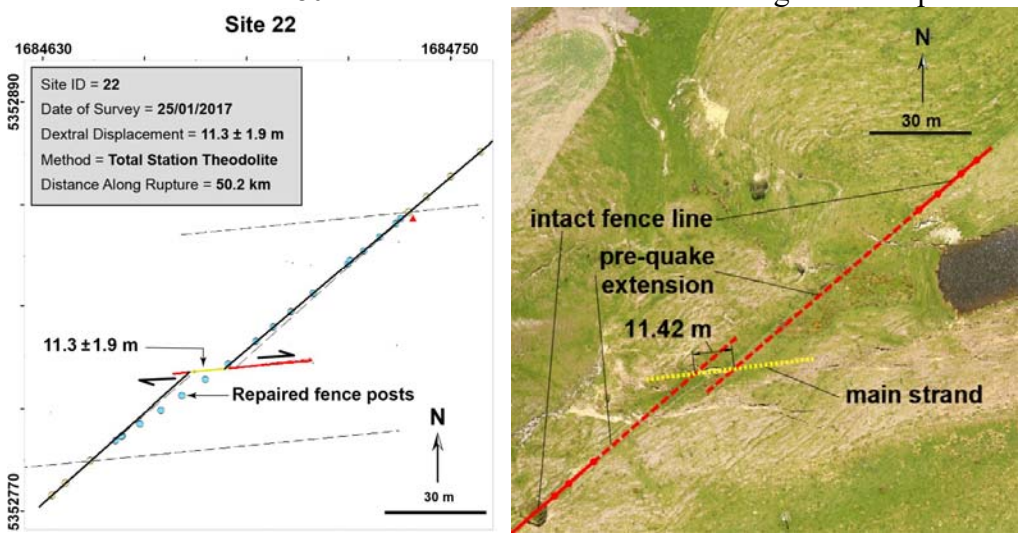


Figure 6. Comparison of field survey using a total Station (left) against Sfm measurements (right). Field survey data from Kearse et al. 2018.

Conclusions

Following the occurrence of the November 14 2016 Kaikoura earthquake in New Zealand, post-earthquake reconnaissance surveys were conducted by the GEER group, GNS and collaborators from the University of Michigan using UAVs. The Structure-from-Motion (SfM) technique was used to map a total 25 sites using 23,172 images covering a plan view area of 7.2 km² with a focus on landslide and fault rupture sites. The data is briefly presented herein with particular emphasis on a section of Kekerengu fault rupture and Limestone Hills landslide. SfM is found to result in high resolution (cm-level ground sampling distance) DSMs that are similar to aerial 1-m LiDAR DSM. For the sites shown, due to its higher resolution compared to the 1 m LiDAR data, and because of the RGB attributes of the pixels in the photogrammetry technique, SfM is found to be particularly valuable in identifying fine features of target sites that are important in post-earthquake performance documentation. Overall, the UAV-enabled SfM approach is found to be successful in covering large areas at high resolutions and in a reliable manner, making it a suitable, and portable, technique for post-earthquake reconnaissance.

Acknowledgements

The work is funded through a NSF RAPID Grant No. EAR-1719496. In addition, data from the December 2016 field expedition is based upon work supported by NSF Grant No. CMMI-1266418 through GEER. Opinions, findings, and conclusions or recommendations are those of the authors and do not necessarily reflect NSF views. Michael Olsen & Matt O'Banion (Oregon State

University) assisted with obtaining coordinates for ground control targets for several landslides.

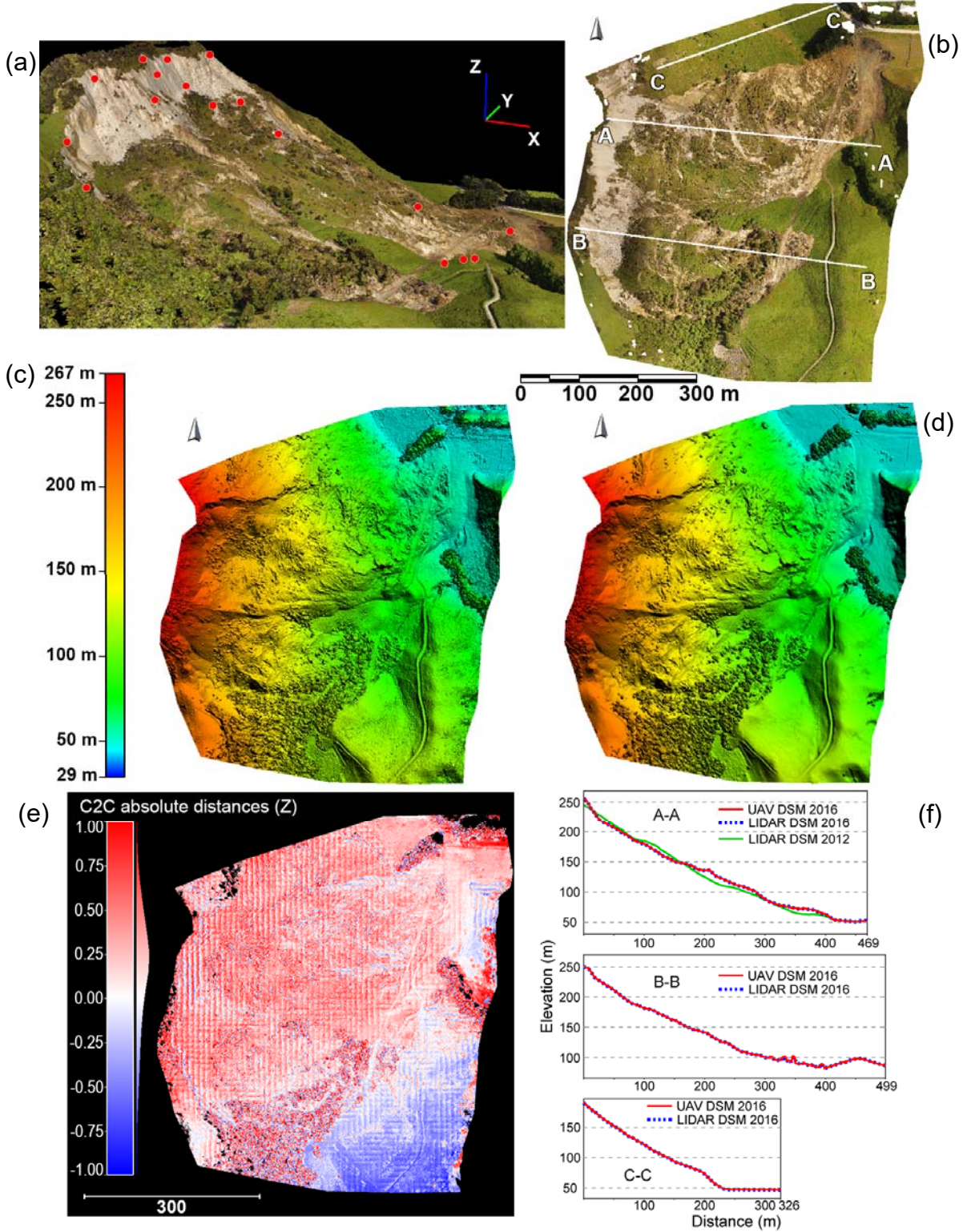


Figure 7. Limestone Hills landslide: (a) Oblique view, (b) orthophoto, and (c) DSM of SfM model; (d) DSM of 2016 LiDAR model; (e) DEM of difference between SfM model and 2016 LiDAR model; (f) indicative cross-sections through the landslide illustrating before (2012 LiDAR model) and after (SfM and 2016 LiDAR).

References

- 1. Dellow, S., Massey, C., Cox, S., Archibald, G., Begg, J., Bruce, Z., Carey, J. Davidson, J., Della Pasqua, F., Glassey, P., Hill, M., Jones, K., Lyndsell, B., Lukovic, B. McColl, S., Rattenbury, M., Read, S., Rosser, B., Singeisen, C. Townsend, D., Villamor, P. Villeneuve2, M., Wartman, J., Rathje, E., Sitar, N., Athanasopoulos-Zekkos A. Manousakis, J., and Little, M., Landslides caused by the Mw 7.8 Kaikoura Earthquake and the immediate response, Bulletin of the New Zealand Society for Earthquake Engineering, 2017, 50 (2), 106-116.
- 2. Franke, K. W., Rollins, K. M., Ledezma, C., Hedengren, J. D., Wolfe, D., Ruggles, S., Bender, C., and Reimschiissel, B. Reconnaissance of Two Liquefaction Sites Using Small Unmanned Aerial Vehicles and Structure from Motion Computer Vision Following the April 1, 2014 Chile. 2016 Earthquake. J. Geotech. Geoenviron. Eng., DOI: 10.1061/(ASCE)GT.1943-5606.0001647.
- 3. GEER, Geotechnical reconnaissance of the 2016 Mw 7.8 Kaikoura, New Zealand earthquake, Version 1.0, June 2017.
- 4. Greenwood, W., Zekkos, D., Clark, M. K., Lynch, J. P., Bateman, J., and Chamlagain, D. UAV-Based 3-D Characterization of Rock Masses and Rock Slides in Nepal. 1016. In 50th US Rock Mechanics/Geomechanics Symposium, Houston, TX.
- Hamling, I.J.; Hreinsdottir, S.; Clark, K.J.; Elliot, J.; Liang, C.; Fielding, E.; Litchfield, N.J.; Villamor, P.; Wallace, L.M.; Wright, T.J.; D'Anastasio, E.; Bannister, S.C.; Burbidge, D.R.; Denys, P.; Gentle, P.; Howarth, J.D.; Mueller, C.; Palmer, N.G.; Pearson, C.; Power, W.L.; Barnes, P.; Barrell, D.J.A.; Van Dissen, R.J.; Langridge, R.M.; Little, T.; Nicol, A.; Pettinga, J.; Rowland, J.; Stirling, M.W. Complex multifault rupture during the 2016 Mw 7.8 Kaikoura earthquake, New Zealand. 2017, Science, 356(6334): eaam7194; doi: 10.1126/science.aam7194.
- Kayen, R., Dashti, S., Kokusho, T., Hazarika, H., Franke, K., Oettle, N., Wham, B., Ramirez, J., Briggs, D., Guillies, S., Cheng, K., Tanoue, Y., Takematsu, K., Matsumoto, D., Morinaga, T., Furuichi, H., Kitano, Y., Tajiri, M., Chaudhary, B., Nishimura, K., Chu, C. Geotechnical Aspects of the 2016 Mw 6.2, Mw 6.0, and Mw 7.0 Kumamoto Earthquakes. 2016 GER Report No. GEER-048, 163 p., http://geerassociation.org/component/geer reports/?view=geerreports&id=75&layout=default.
- 7. Kearse, J., T.A. Little, R. J. Van Dissen, P. M. Barnes, R. Langridge, J. Mountjoy et al. Onshore to offshore ground-surface and seabed rupture of the Jordan-Kekerengu- Needles fault network during the 2016, M w 7.8 Kaikōura earthquake, New Zealand, Bulletin of the Seismological Society of America (Kaikōura earthquake special issue) (accepted).
- 8. Massey, C. I., Townsend, D., Rathje, E., Allstadt, K., Kaneko, Y., Lukovic, B., Bradley, B., Wartman, J., Horspool, N., Hamling, I., Carey, J., Cox, S., Davidson, J., Dellow, S., Godt, J., Holden, C., Jibson, R., Jones, K., Kaiser, A., Little, M. Lyndsell, B., McColl, S., Morgenstern, R., Petley, D. N., Rengers, F., Rhoades, D., Rosser, B., Strong, D., Singeisen, C., Villeneuve, M. Landslides triggered by the MW 7.8 14 November 2016 Kaikoura Earthquake, New Zealand. In review. *Bulletin of the Seismological Society of America*. Kaikoura Earthquake special edition.
- Van Dissen, R. J., T. A. Little, R. M. Burke, P. J. Tonkin, K. P. Norton, S. N. Bacon, R. Bowers, H. L. Goldstein, J. R. Redwine, D. G. Sutherland, S. F. Tillinghast, J. R. Kearse, J. Whattam, D. B. Townsend, A. M. Benson, and N. Wang. Late Quaternary dextral slip rate of the Kekerengu Fault: New Zealand's third fastest on land fault, in Abstracts, GeoSciences 2016, Wanaka, Riesselman, C. and A. Roben (Editors). Geoscience Society of New Zealand Miscellaneous Publication 145A, p. 89.
- 10. Westoby, M. J., Brasington, J., Glasser, N. F., Hambrey, M. J., & Reynolds, J. M. 'Structure-from-Motion' photogrammetry: A low-cost, effective tool for geoscience applications. *Geomorphology*, 2012; **179**: 300-314.
- 11. Zekkos, D., Clark, M., Cowell, K., Medwedeff, W., Manousakis, J, Saroglou, H., Tsiambaos, G. Satellite and UAV-enabled mapping of landslides caused by the November 17th 2015 Mw 6.5 Lefkada earthquake. In 19th International Conference on Soil Mechanics and Geotechnical Engineering, 17-22 September 2017, Seoul, South Korea.